scientific reports

Check for updates

OPEN

FABP4 deficiency ameliorates alcoholic steatohepatitis in mice via inhibition of p53 signaling pathway

Hao Xing[1,2,5], Zhan Wu[1,2,5], Keqing Jiang[1,2,3,4], Guandou Yuan[1,2,3], Zhenya Guo[1,2,3], Shuiping Yu[1,2,4], Songqing He[1,2,3,4]✉ & Fudi Zhong[1,2,3,4]✉

Fatty acid-binding protein 4 (FABP4) plays an essential role in metabolism and inflammation. However, the role of FABP4 in alcoholic steatohepatitis (ASH) remains unclear. This study aimed to investigate the function and underlying mechanisms of FABP4 in the progression of ASH. We first obtained alcoholic hepatitis (AH) datasets from the National Center for Biotechnology Information–Gene Expression Omnibus database and conducted bioinformatics analysis to identify critical genes in the FABP family. We then established ASH models of the wild-type (WT) and *Fabp4*-deficient (*Fabp4*$^{-/-}$) mice to investigate the role of FABP4 in ASH. Additionally, we performed transcriptional profiling of mouse liver tissue and analyzed the results using integrative bioinformatics. The *FABP4*-associated signaling pathway was further verified. *FABP4* was upregulated in two AH datasets and was thus identified as a critical biomarker for AH. *FABP4* expression was higher in the liver tissues of patients with alcoholic liver disease and ASH mice than in the corresponding control samples. Furthermore, the *Fabp4*$^{-/-}$ ASH mice showed reduced hepatic lipid deposition and inflammation compared with the WT ASH mice. Mechanistically, *Fabp4* may be involved in regulating the p53 and sirtuin-1 signaling pathways, subsequently affecting lipid metabolism and macrophage polarization in the liver of ASH mice. Our results demonstrate that *Fabp4* is involved in the progression of ASH and that *Fabp4* deficiency may ameliorate ASH. Therefore, FABP4 may be a potential therapeutic target for ASH treatment.

Keywords FABP4, Alcoholic steatohepatitis (ASH), p53, Bioinformatics analysis

Epidemiological studies revealed that the incidence and prevalence of alcoholic liver disease (ALD) are rapidly increasing worldwide[1]. One of the initial symptoms of ALD is mild alcoholic fatty liver (AFL), which is characterized by slightly abnormal levels of hepatic biochemical and pathological factors. Among the ALD patients with AFL, 10–20% progress to more severe liver diseases, such as alcoholic steatohepatitis (ASH). ASH is characterized by hepatic steatosis and inflammation, with or without liver fibrosis[2]. Although ALD has been extensively studied, its pathogenesis has not yet been fully elucidated. Previous studies found that pro-inflammatory pathways, apoptosis, and immune-related factors are involved in ethanol-induced liver damage. Chronic and excessive consumption of alcohol further aggravates liver damage, leading to alcoholic liver fibrosis, alcoholic cirrhosis, and even hepatocellular carcinoma[3]. Compulsory abstinence from alcohol is the best treatment for ALD patients; however, most ALD patients are unable to effectively quit alcohol[4]. Currently, there are no effective drugs for the clinical treatment of ALD. Therefore, there is an urgent need to identify novel therapeutic targets and develop therapeutic interventions for ALD.

The fatty acid-binding proteins (FABPs) are a family of nine homologous intracellular lipid-binding proteins that regulate lipid trafficking and metabolism and have specific tissue distribution patterns[5,6]. FABP4 is predominantly expressed in adipocytes and macrophages and plays an essential regulatory role in energy metabolism

[1]Division of Hepatobiliary Surgery, The First Affiliated Hospital of Guangxi Medical University, Nanning 530021, China. [2]Guangxi Key Laboratory of Immunology and Metabolism for Liver Diseases, Nanning 530021, China. [3]Key Laboratory of Early Prevention and Treatment for Regional High Frequency Tumor (Guangxi Medical University), Ministry of Education, Nanning 530021, China. [4]Guangxi Key Laboratory of Basic and Clinical Application Research for Hepatobiliary Diseases, Nanning 530021, Guangxi, China. [5]These authors contributed equally: Hao Xing and Zhan Wu. ✉email: dr_hesongqing@163.com; andy020@126.com

and inflammatory response[7]. Several studies demonstrated that ethanol metabolism promotes the expression of FABP4 in the liver[8–10], indicating that FABP4 is associated with ALD progression. However, the function and underlying mechanism of FABP4 in the progression of ASH remain unclear.

In this study, we hypothesized that FABP4 may have an essential role in hepatic lipid metabolism and inflammation in ASH. Therefore, we conducted a bioinformatics analysis of Gene Expression Omnibus (GEO) data to analyze the role of FABP4 in ethanol-induced ASH. Furthermore, we explored the underlying molecular mechanism of FABP4 in ASH mice.

Materials and methods

Dataset collection

The microarray datasets GSE142530, GSE167308, and GSE73173 were downloaded from the National Center for Biotechnology Information–GEO database. The GSE142530[11] dataset (based on the GPL11154 platform) consisted of 10 samples from alcoholic hepatitis (AH) patients and 11 samples from healthy individuals. The GSE167308[12] dataset (based on the GPL20321 platform) comprised 7 samples from AH patients and 5 samples from healthy individuals. The GSE73173[13] dataset consisted of the gene expression profile of RAW264.7 macrophages subjected to exogenous FABP4 treatment. Quality control analysis and microarray data pre-processing, including background correction and normalization, were performed in the R software (v4.3.2, https://www.r-project.org/) using the Bioconductor package before formal analysis.

Identification of differentially expressed genes (DEGs)

DEGs were identified using the R Bioconductor package limma (v3.54.2). The *P*-values were adjusted based on Benjamini–Hochberg's false discovery rate (FDR), and genes with the *P*-value of < 0.05 and $|\text{Log2 fold change (log2FC)}| \geq 0.585$ were defined as DEGs. Volcano plots were generated using the R ggplot2 package (v3.4.1), heatmaps for DEGs from each dataset were plotted using the R Pheatmap package (v1.0.12), and Venn diagrams were generated using the R VennDiagram package (v1.7.3).

Functional enrichment analysis of DEGs

Functional enrichment analysis of DEGs was conducted using the R clusterProfiler package (v4.6.2) and the GO plot package (v1.0.2) at a *P*-value of < 0.05. All DEGs were subjected to gene set enrichment analysis (GSEA), gene ontology (GO) analysis (biological process, BP; cellular component, CC; and molecular function, MF), and Kyoto Encyclopedia of Genes and Genomes (KEGG) pathway enrichment analysis. Additionally, the up- and downregulated DEGs were subjected to GO enrichment analysis.

Screening and validation of critical gene signatures

Weighted gene co-expression network analysis (WGCNA) was conducted using the default recommended parameters to determine the relationship between *FABP4* and AH using the R WGCNA package (v1.72-1). The diagnostic value of *FABP4* for AH was determined by generating receiver operating characteristic (ROC) curves and calculating the area under the curve (AUC) values using the R pROC package (v1.18.0). A two-sided *P*-value of < 0.05 was considered statistically significant. Furthermore, the random forests (RF), support vector machine (SVM), and eXtreme Gradient Boosting (XGBoost) algorithms were used to calculate the AUC values for AH using the R mlr3 package (v0.15.0).

Evaluation and correlation analysis of infiltrated immune cells

CIBERSORT was used to analyze the infiltration of 22 and 25 types of immune cells in humans and mice, respectively. The relative abundance of infiltrated immune cells was determined at $P < 0.05$. The correlation heatmap of infiltrated immune cells was plotted using the R corrplot package (v0.92). Wilcoxon rank-sum test was used to determine the differential immune cell infiltration between the AH and control groups, and Spearman's correlation test was used to analyze the relationship between the biomarkers and infiltrating immune cells. The results were visualized using the R ggcorrplot package (v0.1.4).

Animal models

The present study was conducted in compliance with the ARRIVE guidelines. Female wild-type (WT) and FBAP4$^{-/-}$ C57BL/6 mice were purchased from GemPharmatech (Jiangsu, China). The *Fabp4*$^{-/-}$ mice were generated using the Clustered Regularly Interspaced Short Palindromic Repeats/CRISPR-associated protein 9 technology[14]. All mice were maintained in a specific pathogen-free facility at Guangxi Medical University (Guangxi, China). The Lieber–Decarli liquid diet (LD; Trophic Animal Feed High-tech Co. Ltd., Jiangsu, China) containing 5% v/v ethanol was used to establish a standardized murine ASH model based on the Gao-Binge model[15]. The feeding protocol can be extended to long-term feeding, up to 8 weeks, plus a single ethanol binge based on body weight. WT mice (8–12 weeks old) were given the control Lieber–Decarli liquid diet (CD-fed) and the ethanol Lieber–Decarli liquid diet (EtOH-fed). In addition, WT and *Fabp4*$^{-/-}$ mice (8–12 weeks old) were used to generate the ASH model. The mice were anesthetized using isoflurane (RWD Life Science Co., Ltd., Shenzhen, China) via inhalation, 8 h after the last ethanol gavage, and their retro-orbital blood and liver tissues were collected for subsequent analysis. All animal experiments were approved by the Animal Care and Use Committee of Guangxi Medical University.

Patient samples

Liver tissue samples were obtained from healthy individuals and clinically confirmed ALD patients admitted to the Guangxi Medical University Hospital. The healthy liver tissue was obtained from donated liver or pathological specimens of benign liver diseases (such as liver hemangioma). The use of liver tissue samples was approved by the Ethics Committee of the First Affiliated Hospital of Guangxi Medical University (No.2024-E456-01). All the samples were analyzed in accordance with the Declaration of Helsinki, and all patients provided informed written consent for the purpose of the research.

Serum biochemical analysis

The serum levels of alanine aminotransferase (ALT), aspartate aminotransferase (AST), triglyceride (TG), and total cholesterol (TC) were measured using an autoanalyzer (Catalyst one, IDEXX, USA). Serum FABP4 levels were measured using commercially available ELISA kits (Meimian Industrial Co., Jiangsu, China) following the manufacturer's instructions.

Tissue biochemical analysis

The TG and TC levels in liver tissue homogenates were detected using the TG (#A110-1-1) and TC (#A111-1-1) assay kits (Jiancheng Institution PeproTech, Jiangsu, China), respectively, according to the manufacturer's instructions. Hepatic tumor necrosis factor (TNF)-α and interleukin (IL)-1β levels were measured using commercially available ELISA kits (Thermo Fisher Scientific, Waltham, MA, USA).

Histopathologic and immunohistochemical analyses

Fresh liver tissue samples were frozen, sliced into 8-μm-thick sections, and treated with oil red O stain. The resected liver tissue samples were fixed overnight in 10% neutral-buffered formalin solution, embedded in paraffin, and sectioned into 5-μm-thick sections. The sections were then dewaxed with xylene, dehydrated with alcohol, placed in sodium citrate buffer (pH 6), and heated in a microwave for 5 min for antigen retrieval. The sections were stained with hematoxylin and eosin (H&E), and the histopathological alterations in the liver biopsies were observed using a slide scanner (NanoZoomer S60; Hamamatsu Photonics, Japan) at 100×.

The tissue sections were incubated with 3% hydrogen peroxide for 10 min to eliminate endogenous peroxidase activity. Thereafter, the sections were incubated with goat anti-F4/80 antibodies (1:500; Cell Signaling Technology, Danvers, MA, USA) and anti-CD206 antibodies (1:300; Cell Signaling Technology) for 2 h at room temperature, followed by anti-goat ImmPRESS kit (Vector Laboratories), according to the manufacturer's instructions. The images were collected using the NanoZoomer S60 scanner (Hamamatsu, Japan). The pathological severity of histopathologic and immunohistochemical sections were by using Image J (v1.46r, https://imagej.nih.gov/ij/) to quantitatively assess.

Quantitative reverse transcription-polymerase chain reaction (qRT-PCR)

Total RNA from frozen liver tissues (0.1 g) was extracted using TRIzol (15596026, Invitrogen, Carlsbad, CA, USA), according to the manufacturer's instructions. The cDNA was synthesized using the RevertAid First Strand cDNA Synthesis Kit (K1622, Thermo Fisher Scientific). The qRT-PCR assay was conducted using a SYBR Green PCR master mix (1725125, Bio-Rad) on a real-time PCR system (CFX 96 Touch, Bio-Rad). The primers used for the qRT-PCR assay are provided in Table S1. Glyceraldehyde 3-phosphate dehydrogenase (GAPDH) was used to normalize the gene expression.

Western blot analysis

Total protein from the liver tissue samples was extracted using radio-immunoprecipitation assay lysis buffer (P0013B, Beyotime, Shanghai, China) and quantified using a bicinchoninic acid assay kit (Beyotime). The protein samples were separated using sodium dodecyl sulfate–polyacrylamide gel electrophoresis and transferred to a 0.45-μm polyvinylidene fluoride (PVDF) membrane (Merck KGaA, Darmstadt, Germany). The PVDF membranes were then blocked with 5% milk and washed thrice with Tris-buffered saline containing 0.1% Tween-20 (TBST) for 10 min each. The membranes were incubated overnight with primary antibodies at 4 °C and washed thrice with TBST for 10 min each. The membranes were then incubated with HRP-labeled goat anti-rabbit/mouse IgG (1:1000; Proteintech, Wuhan, China). The protein bands were detected using the ECL chemiluminescent kit (Epizyme, Shanghai, China), and the band densities were analyzed using the ImageJ software. The following primary antibodies were used in this study: anti-FABP4 (12802-1-AP), anti-p53 (10442-1-AP), anti-CASP3 (25128-1-AP), anti-BCL-2 (26593-1-AP), anti-BAX (50599-2-Ig), anti-PI3K (20584-1-AP), anti-NF-κB (10745-1-AP), anti-PPARα (66826-1-Ig), anti-AKT (60203-2-Ig), anti-P-AKT (80455-1-RR), anti-AMPK (10929-2-AP), anti-CPT-1 (15184-1-AP), anti-SREBP1 (14088-1-AP), and anti-SCD-1 (28678-1-AP), purchasing from Proteintech (Wuhan, China); anti-F4/80 (70076T), anti-NLRP3 (15101S), anti-CASP1 (24232S), anti-IL-1β (12242T), anti-SIRT1 (2028S), anti-IKK (61294S), anti-ACC (3676T), anti-FASN (3180T), anti-CD206 (#24595), anti-P-IRS-1 (636) (#2388), anti-P-IRS-1(307) (#2381), anti-IRS-1 (#2382), anti-P-PI3K (#17366), anti-P-AMPK (#50081), anti-P-ACC (#3661), anti-P-IKK (#2078), anti-P-NF-κB (#3033), and anti-GAPDH (2118T), purchasing from Cell Signaling Technology (Danvers, Massachusetts, USA). GAPDH was used to normalize the protein expression signals.

Transcriptional profiling

Total RNA was extracted from the flash-frozen liver tissues of the control and ASH *Fabp4*$^{-/-}$ mice using TRIzol reagent (Invitrogen). The quality of the RNA samples was evaluated using the NanoDrop 2000c

spectrophotometer (Thermo Fisher Scientific) and a bioanalyzer (Agilent). Sequencing libraries were generated by reverse transcription-polymerase chain reaction (RT-PCR) amplification and sequenced on the HiSeq 2500 sequencing system (RIBOBIO, Guangzhou, China).

Statistical analysis

The statistical and data analyses were performed utilizing R software. Normally distributed continuous variables were expressed as the mean ± standard deviation (SD). Two groups were compared using a two-tailed Student's *t*-test. A two-sided *P*-value of < 0.05 was considered statistically significant.

Ethics statement

The Ethics Committee of the First Affiliated Hospital of Guangxi Medical University approved the protocol (No. 2024-E456-01), which was conducted according to the Declaration of Helsinki. All included patients provided informed written consent for the purpose of the research.

Results

DEGs in AH datasets and single-gene GSEA of *FABP4*

A total of 3749 (1872 downregulated and 1877 upregulated) and 6038 (3202 downregulated and 2836 upregulated) DEGs were identified in the GSE142530 and GSE167308 datasets, respectively (Fig. 1A–D). Among these, 2201 overlapping DEGs (1094 downregulated and 1107 upregulated) related to AH were identified between the two datasets, as shown in the Venn diagram (Fig. 1E). Further analysis revealed that three upregulated DEGs in the GSE142530 dataset and one upregulated and two downregulated DEGs in the GSE167308 dataset belonged the *FABP* family (Fig. 1F,G). *FABP4* was upregulated in both the AH datasets (Fig. 1F,G). Single-gene GSEA showed that *FABP4* was primarily involved in lipid metabolism, immunity, and inflammation-associated pathways, including regulation of lipolysis in adipocytes, PI3K-AKT signaling pathway, Wnt signaling pathway, MAPK signaling pathway, chemokine signaling pathway, and inflammatory mediator regulation of TRP channels (Fig. 1H–M).

Verification of *FABP4* in AH datasets and expression of *FABP4* in ALD patients

The two AH datasets were combined, and the batch effects were removed by the R sva package (v3.46.0)[16]. The results of WGCNA revealed the presence of 13 co-expression modules in the AH datasets (Fig. 2A–C). Module–trait correlation analysis showed that the turquoise and salmon modules were associated with AH and that the association between the turquoise module and AH was more significant (Fig. 2D). Further screening revealed the presence of *FABP4* in the turquoise module (Fig. 2E). The AUC of the generated ROC curve for the *FABP4* predictive values in AH was 0.82 (Fig. 2F). Furthermore, the AUCs for *FABP4* with RF, SVM, and XGBoost algorithms were 0.83, 0.80, and 0.77, respectively (Fig. 2G), confirming that *FABP4* had high predictive accuracy. Analysis of *FABP4* expression in the AH datasets showed that *FABP4* expression was upregulated in the AH samples compared with that in the control samples in both the GSE142530 and GSE167308 datasets ($P < 0.05$, Fig. 2H,I). Furthermore, qRT-PCR and WB assays showed that hepatic FABP4 mRNA and protein levels were increased in ALD patients compared with those in healthy individuals (Fig. 2J,K). These results indicate that *FABP4* is significantly elevated in the liver tissues of ALD patients.

Expression of *Fabp4* in the liver tissues of ASH mice

We further conducted biochemical, histopathologic, and immunohistochemical analyses of the EtOH-fed and CD-fed WT mouse models. The results of H&E and oil red O staining showed that the EtOH-fed mice had a higher degree of liver injury and lipid deposition than the CD-fed mice (Fig. 3A). Additionally, the EtOH-fed mice had higher serum levels of ALT, AST, TG, and TC than the CD-fed mice (Fig. 3B–E). Moreover, the EtOH-fed mice showed higher hepatic levels of TNF-α, IL-6, TG, and TC than the CD-fed mice (Fig. 3F–I). Furthermore, the EtOH-fed mice had higher *Fabp4* mRNA and protein levels in the liver tissues than the CD-fed mice (Fig. 3J,K). Interestingly, serum FABP4 levels showed no significant difference between the EtOH-fed and CD-fed mice (Fig. S1). These results indicate that *Fabp4* expression was elevated in the liver tissues of ASH mice.

Fabp4 deficiency reduced hepatic lipid deposition and liver injury in ASH mice

To further explore the role of *Fabp4* in ASH progression, we conducted biochemical, histopathologic, and immunohistochemical analyses of the EtOH-fed WT and *Fabp4*$^{-/-}$ mice. The genotype verification of the *Fabp4*$^{-/-}$ mice is shown in Fig. S2. The results of ELISA, qRT-PCR, and WB showed almost no expression of *Fabp4* in the serum and liver tissues of the EtOH-fed *Fabp4*$^{-/-}$ mice (Fig. 4A–C). The results of H&E and oil red O staining showed that the EtOH-fed *Fabp4*$^{-/-}$ mice showed reduced liver injury levels and lipid deposition compared with the EtOH-fed WT mice (Fig. 4D). Additionally, the EtOH-fed *Fabp4*$^{-/-}$ mice showed decreased serum ALT and AST levels compared with the EtOH-fed WT mice (Fig. 4E,F). Moreover, the EtOH-fed *Fabp4*$^{-/-}$ mice showed decreased hepatic levels of TG, TC, TNF-α, and IL-6 compared with the EtOH-fed WT mice (Fig. 4G–J). These results indicate that *Fabp4* deficiency may ameliorate hepatic lipid deposition and liver injury in ASH mice.

Transcriptional profiling of the liver tissue from WT and *Fabp4*$^{-/-}$ ASH mice and bioinformatics analysis

To further investigate the mechanisms of *Fabp4* in the development of ASH, we performed transcriptional profiling of the liver tissues of ASH mice. A total of 964 (359 downregulated and 605 upregulated) DEGs were identified in the liver tissues of the WT and *Fabp4*$^{-/-}$ mice (Fig. 5A,B). The top 50 (30 upregulated and 20

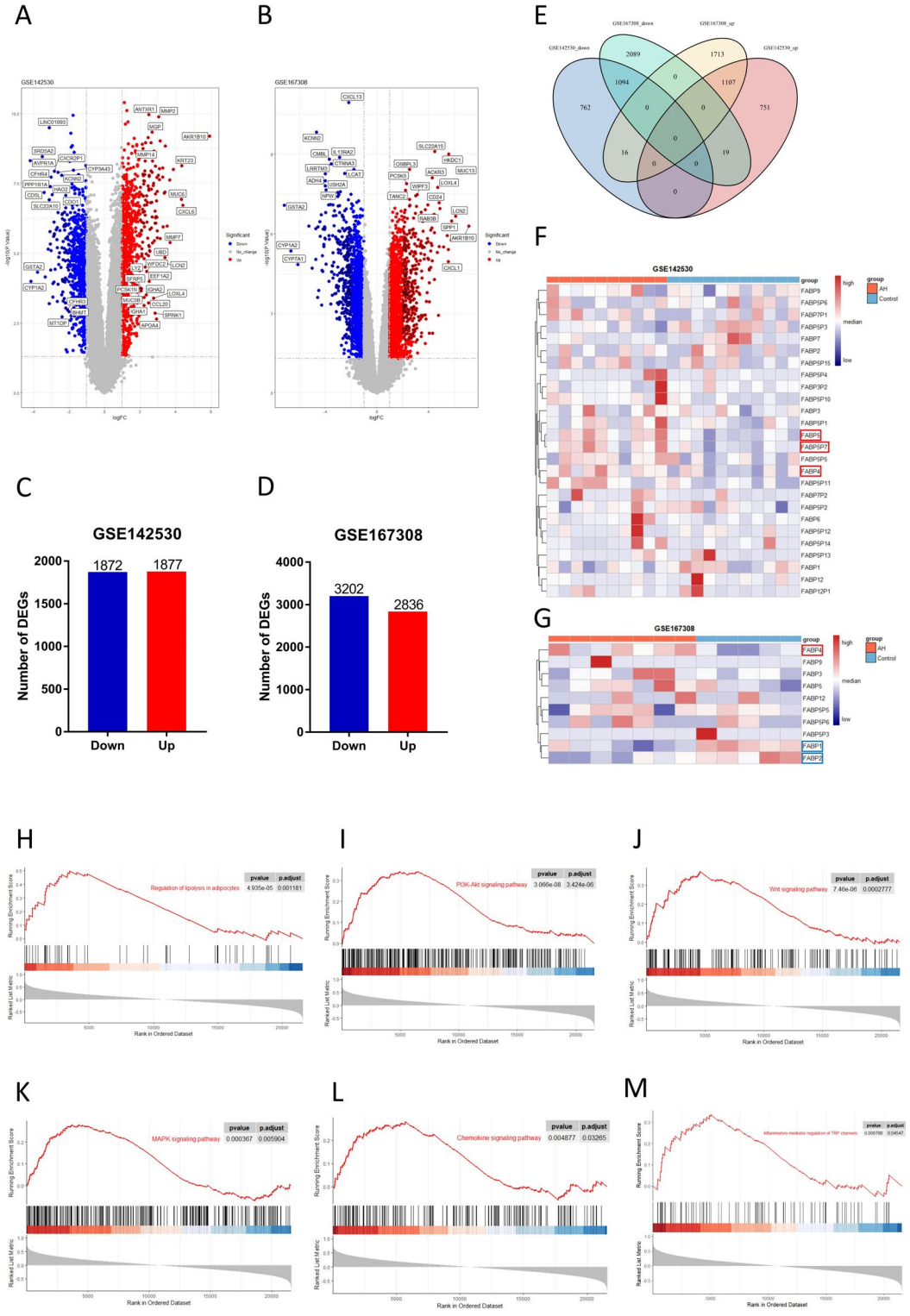

Fig. 1. Differential gene expression analysis of the GSE142530 and GSE167308 datasets and single-gene GSEA of *FABP4*. (**A**,**B**) Volcano plots of the DEGs in the GSE142530 (**A**) and GSE167308 (**B**) datasets. (**C**,**D**) Number of DEGs in the GSE142530 (**C**) and GSE167308 (**D**) datasets. (**E**) Venn diagram of the DEGs in the GSE142530 and GSE167308 datasets. (**F**,**G**) Heatmaps of the *FABP* family-related DEGs in the GSE142530 (**F**) and GSE167308 (**G**) datasets. (**H**–**M**) Single-gene GSEA profiles depicting the six significant GSEA sets in AH. Results are presented as the mean ± SD.

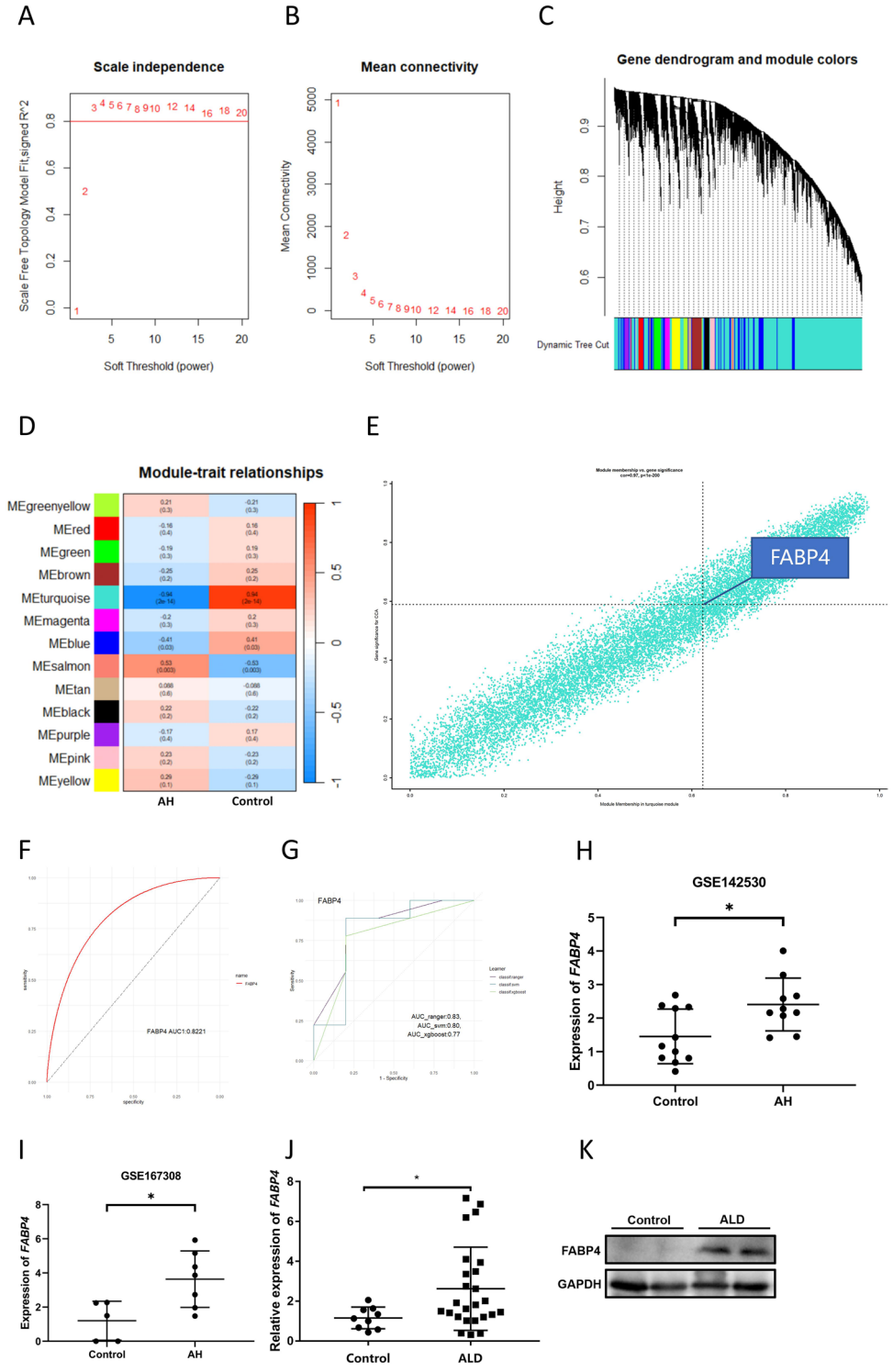

Fig. 2. Correlation analysis between *Fabp4* expression and AH and verification of *Fabp4* expression in ALD patients. (**A**–**E**) WGCNA of the combined datasets (GSE142530 and GSE167308). (**F**) AUC of the ROC curve for the *FABP4* predictive values in AH. (**G**) AUCs for *FABP4* in AH with RF, SVM, and XGBoost algorithms. (**H**,**I**) *Fabp4* expression in the GSE142530 (**H**) and GSE167308 (**I**) datasets. (**J**–**K**) Hepatic mRNA (**J**) and protein (**K**) levels of *FABP4* in ALD patients. Results are presented as the mean ± SD. $^{*}P < 0.05$.

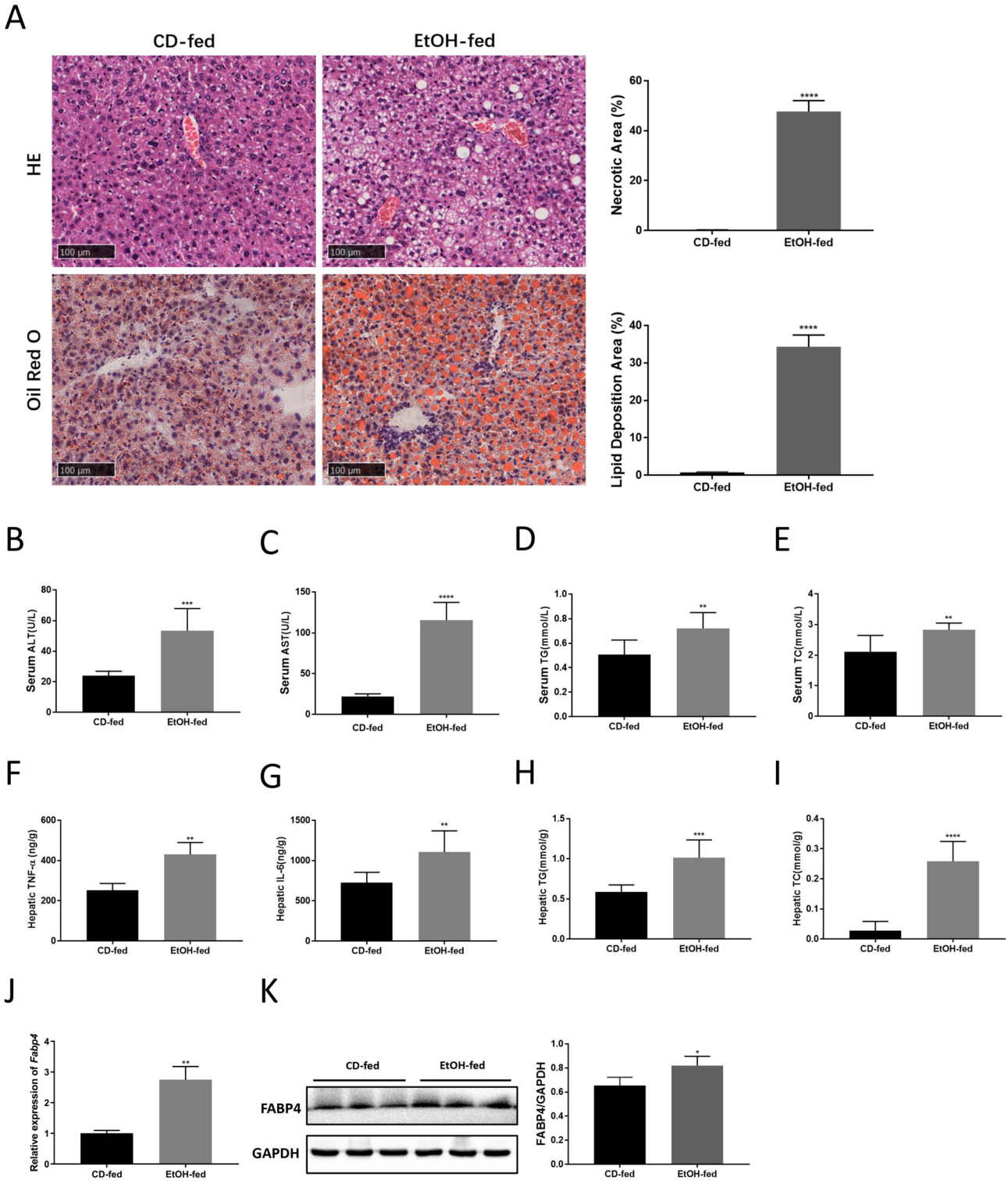

Fig. 3. Biochemical, histopathologic, and immunohistochemical analyses of the CD-fed and EtOH-fed WT mouse models. (**A**) H&E and oil red O staining of the liver tissue sections of the CD-fed and EtOH-fed WT mice (scale bar, 100 μm). (**B**–**E**) Serum levels of ALT (**B**), AST (**C**), TG (**D**), and TC (**E**) in the CD-fed and EtOH-fed WT mice. (**F**–**I**) Hepatic levels of TNF-α (**F**), IL-6 (**G**), TG (**H**), and TC (**I**) in the CD-fed and EtOH-fed WT mice. (**J**) Hepatic mRNA levels of *Fabp4* in the CD-fed and EtOH-fed WT mice. (**K**) Hepatic protein levels of FABP4 in the CD-fed and EtOH-fed WT mice. Results are presented as the mean ± SD. $^{*}P < 0.05$, $^{**}P < 0.01$, and $^{***}P < 0.001$.

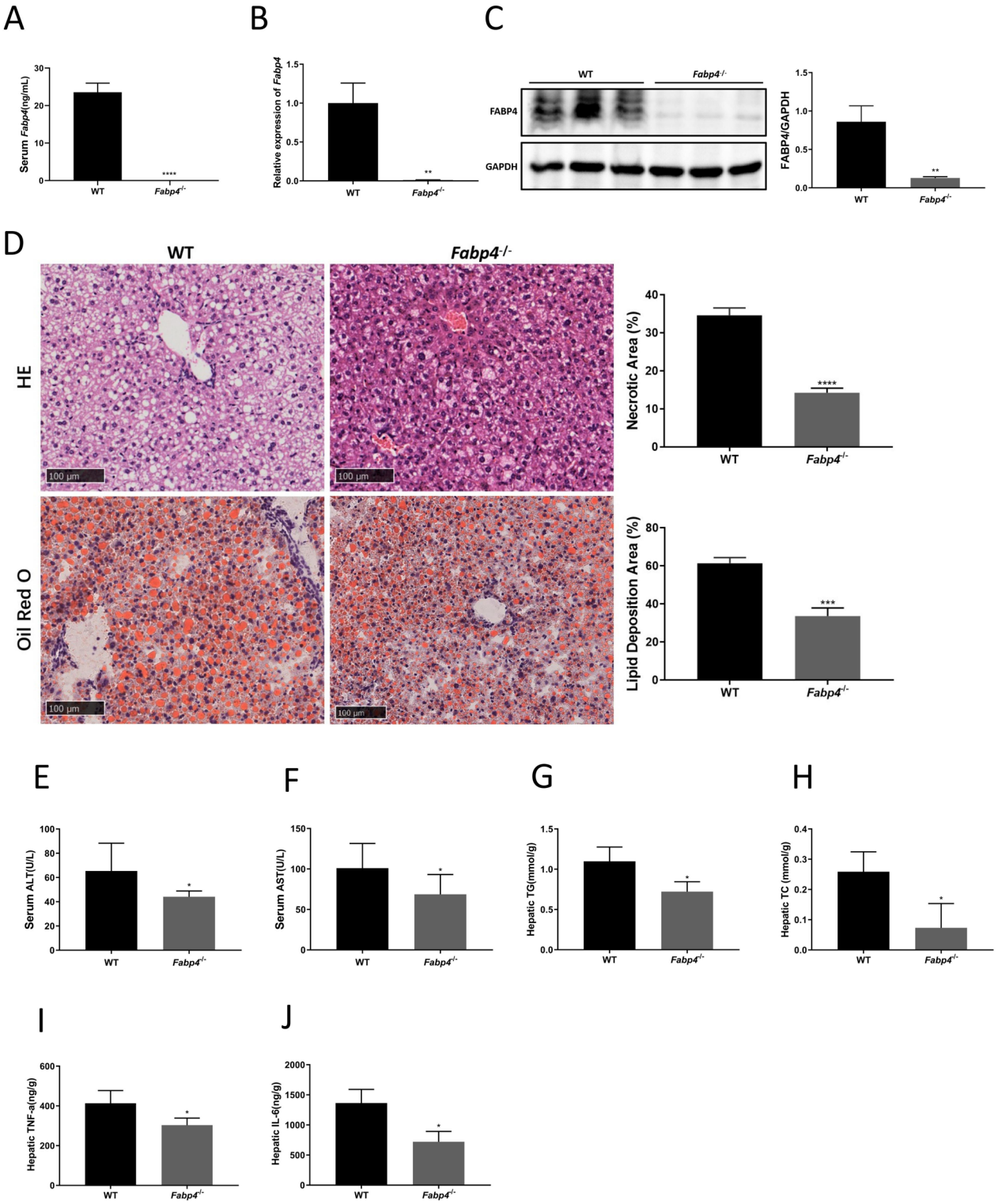

Fig. 4. Biochemical, histopathologic, and immunohistochemical analyses of the EtOH-fed WT and *Fabp4*$^{-/-}$ mouse models. (**A**) Serum levels of FABP4 in the EtOH-fed WT and *Fabp4*$^{-/-}$ mice. (**B**) Hepatic mRNA levels of *Fabp4* in the EtOH-fed WT and *Fabp4*$^{-/-}$ mice. (**C**) Hepatic protein levels of FABP4 in the EtOH-fed WT and *Fabp4*$^{-/-}$ mice. (**D**) H&E and oil red O staining of the liver tissue sections of the EtOH-fed WT and *Fabp4*$^{-/-}$ mice (scale bar, 100 μm). (**E**,**F**) Serum levels of ALT (**E**) and AST (**F**) in the EtOH-fed WT and *Fabp4*$^{-/-}$ mice. (**G**–**J**) Hepatic levels of TG (**G**), TC (**H**), TNF-α (**I**), and IL-6 (**J**) in the EtOH-fed WT and *Fabp4*$^{-/-}$ mice. Results are presented as the mean ± SD ($n = 6$/group). $^{*}P < 0.05$, $^{**}P < 0.01$, and $^{***}P < 0.001$.

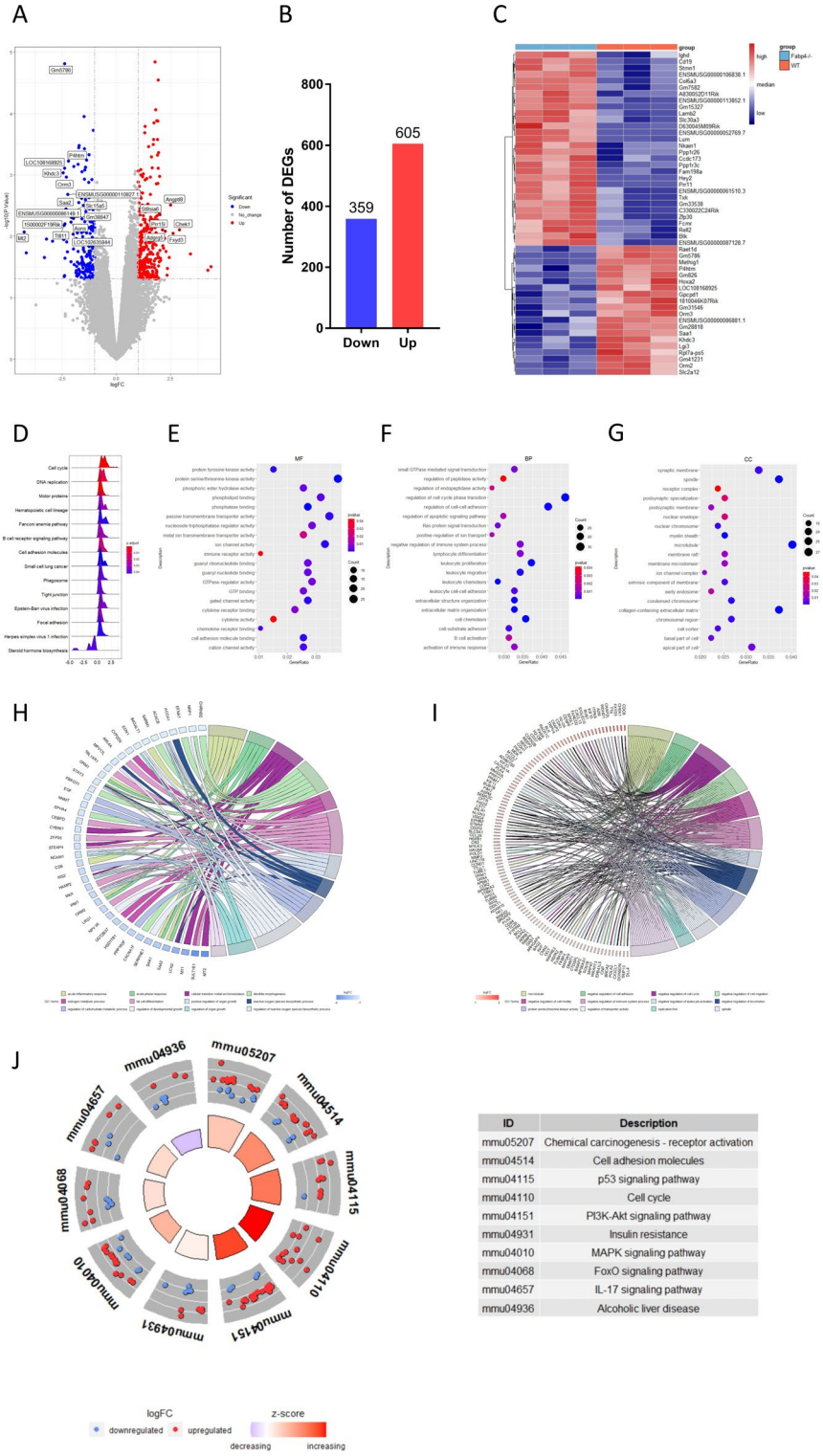

ID	Description
mmu05207	Chemical carcinogenesis - receptor activation
mmu04514	Cell adhesion molecules
mmu04115	p53 signaling pathway
mmu04110	Cell cycle
mmu04151	PI3K-Akt signaling pathway
mmu04931	Insulin resistance
mmu04010	MAPK signaling pathway
mmu04068	FoxO signaling pathway
mmu04657	IL-17 signaling pathway
mmu04936	Alcoholic liver disease

Fig. 5. Transcriptional profiling and bioinformatics analysis of the liver tissues of the EtOH-fed WT and *Fabp4*$^{-/-}$ mice. (**A**) Volcano plots of the DEGs in the liver tissues of the EtOH-fed WT and *Fabp4*$^{-/-}$ mice. (**B**) Number of DEGs in the liver tissues of the EtOH-fed WT and *Fabp4*$^{-/-}$ mice. (**C**) Heatmaps of the top 50 DEGs in the liver tissues of the EtOH-fed WT and *Fabp4*$^{-/-}$ mice. (**D**) GSEA profiles depicting the 14 significant GSEA sets in the EtOH-fed WT and *Fabp4*$^{-/-}$ mice. (**E**–**G**) Bubble charts showing the GO-enriched MF (**E**), *BP* (**F**), and CC (**G**) terms of the DEGs in the EtOH-fed WT and *Fabp4*$^{-/-}$ mice. (**H**,**I**) Chord plots showing the GO-enriched items of the downregulated (**H**) and upregulated (**I**) DEGs in the EtOH-fed WT and *Fabp4*$^{-/-}$ mice. (**J**) Circle plot showing the KEGG-enriched terms of the DEGs in the EtOH-fed WT and *Fabp4*$^{-/-}$ mice.

downregulated) DEGs are presented in heatmaps in Fig. 5C. GSEA showed that the DEGs were significantly enriched in cell cycle, DNA replication, cell adhesion molecules, B cell receptor signaling pathway, focal adhesion, and phagosome (Fig. 5D).

The GO enrichment analysis showed that the DEGs were significantly enriched in cell chemotaxis, regulation of cell cycle phase transition, leukocyte chemotaxis, negative regulation of cell cycle process, and negative regulation of cell cycle phase transition in the MF category (Fig. 5E); spindle pole, microtubule, collagen-containing extracellular matrix, myelin sheath, and replication fork in the BP category (Fig. 5F); and tau protein binding, phosphatase binding, protein serine/threonine kinase activity, extracellular matrix structural constituent, and transmembrane-ephrin receptor activity in the CC category (Fig. 5G). The GO functional enrichment analysis showed that the downregulated DEGs were significantly enriched in acute inflammatory response, acute-phase response, reactive oxygen species biosynthetic process, and fat cell differentiation (Fig. 5H), while the upregulated DEGs were enriched in the negative regulation of cell adhesion, cell cycle, immune system process, and leukocyte activation (Fig. 5I). Lastly, the KEGG pathway enrichment analysis showed that the DEGs were significantly enriched in cell adhesion molecules, p53 signaling pathway, cell cycle, insulin resistance, PI3K-AKT signaling pathway, IL-17 signaling pathway, and ALD (Fig. 5J).

Fabp4 deficiency attenuated the progression of ASH in mice via the p53 signaling pathway

Transcriptional profiling and integrative bioinformatics analyses showed that *Fabp4* was associated with the p53 signaling pathway, insulin resistance, and the PI3K-AKT signaling pathway (Fig. 5J). Therefore, we measured the critical factors in these pathways. The hepatic p53 level was significantly reduced in the EtOH-fed *Fabp4*$^{-/-}$ mice compared with that in the EtOH-fed WT mice (Fig. 6A). Further evaluation of the p53 pathway-associated molecules, such as CASP3, BAX, and BCL-2, showed that the protein levels of CASP3 and BAX (related to apoptosis) were decreased, while that of BCL-2 (related to anti-apoptosis) was increased in the EtOH-fed *Fabp4*$^{-/-}$ mice (Fig. 6A). Additionally, the mRNA levels of *Irs-1*, *Pi3k*, and *Akt* and the protein levels of P-IRS1 (IRS1-636 and IRS1-307), P-PI3K, and P-AKT (associated with alleviating insulin resistance) were increased in the EtOH-fed *Fabp4*$^{-/-}$ mice (Fig. 6B,C). Altogether, these results demonstrate that *Fabp4* may regulate the p53 and insulin/PI3K/AKT signaling pathway in ASH mice.

Previous studies have shown that the inhibition of p53 can upregulate hepatic SIRT1 expression[17–19]. Therefore, qRT-PCR and WB were used to detect the expression of SIRT1 in ASH mice. The results showed that the hepatic SIRT1 mRNA and protein levels were significantly increased in the EtOH-fed *Fabp4*$^{-/-}$ mice (Fig. 6D,E). Furthermore, qRT-PCR analysis showed that in the EtOH-fed *Fabp4*$^{-/-}$ mice, the expression of lipid catabolism-related genes *Pparα*, *Ampk*, and *Cpt-1* was increased, while the expression of lipid anabolism-related genes *Acc*, *Srebf1*, *Scd1*, and *Fasn* was decreased (Fig. 6F,H). Similarly, WB analysis showed that in the EtOH-fed *Fabp4*$^{-/-}$ mice, the expression of P-AMPK, CPT-1, and PPARα was increased, while the expression of P-ACC, SREBP1, SCD1, and FASN was decreased (Fig. 6G,I). These results indicate that *Fabp4* deficiency may inhibit fatty acid synthesis and promote fatty acid oxidation in ASH mice through the p53 and SIRT1 signaling pathways.

Previous studies reported that SIRT1 inhibits the expression of inflammatory factors, such as TNF-α, IL-1β, and IL-6, by directly inhibiting the NF-κB signaling pathway[20]. Therefore, we detected the hepatic expression of NF-κB pathway-related factors using qRT-PCR and WB assays. The results showed that the mRNA and phosphorylated protein expression levels of IKK and NF-κB were decreased in the EtOH-fed *Fabp4*$^{-/-}$ mice (Fig. 6J,K). These results suggest that *Fabp4* deficiency may reduce hepatic inflammation in ASH mice by regulating the SIRT1 signaling pathway.

Fabp4 affected the proportion of macrophage M1/M2 and the expression of pro-inflammatory factors in ASH

Previous studies have found that immune system activation can accelerate AH progression[21,22]. Therefore, we explored the association between *FABP4* expression and immune cell infiltration in AH. CIBERSORT analysis of the immune cell phenotypes in the GSE142530 dataset revealed that compared with the M2 macrophage levels in the control samples, those in the AH samples were lower and negatively correlated with *FABP4* expression (Fig. S3A–D). To further explore the effects of *Fabp4* in macrophages, we conducted GSEA of the DEGs in GSE73173. The results showed that the effects of exogenous *Fabp4* in RAW264.7 macrophages were primarily associated with immunity, inflammation, and lipid metabolism (Fig. S3E–I).

FABP4 is highly expressed in macrophages, especially during the activation of inflammatory response[23,24]. CIBERSORT analysis of 25 immune cell phenotypes in the liver tissues of the WT and *Fabp4*$^{-/-}$ mice revealed that the *Fabp4*$^{-/-}$ mice had a significantly lower proportion of M1 macrophages ($P < 0.01$) and a higher proportion of M2 macrophages than the WT mice. Interestingly, the WT mice showed no M2 macrophage infiltration, while the *Fabp4*$^{-/-}$ mice showed 6% M2 macrophage infiltration (Fig. 7A,B). The correlation heatmap of 23 immune cell types showed that the macrophage levels were significantly correlated with some immune cells (Fig. 7C). We then conducted a correlation analysis between essential genes and infiltrated immune cells in ASH. The results showed that *p53*, *Nlrp3*, *Il-1β*, and *Cxcl-1* were positively correlated with M1 macrophages ($r = 0.66$, 0.6, 0.6, and 0.83, respectively; $P < 0.05$) (Fig. 7D), while *Fabp4* and *Sirt1* were negatively correlated with M2 macrophages ($r = -0.52$) and mast cells ($r = -0.65$, $P < 0.001$), respectively (Fig. 7D). Therefore, we investigated the relationship between *Fabp4* expression and macrophages in the ASH mouse model. The results of immunohistochemistry and WB analyses showed that the *Fabp4*$^{-/-}$ mice had lower F4/80 levels but higher CD206 levels than the WT mice (Fig. 7E,F). Furthermore, the results of the qRT-PCR assay showed that the expression of inflammation-related genes *Tnf-α*, *Il-6*, *Il-1β*, *Il-8*, *Trailr1*, *Iy6g*, *Mcp-1*, and *Cxcl-1* was downregulated in the *Fabp4*$^{-/-}$ mice compared with that in the WT mice (Fig. 7G). Meanwhile, the results of WB analysis showed that the expression of NLRP3, CASP1, pro-IL-1β, and IL-1β proteins was decreased in the *Fabp4*$^{-/-}$ mice compared with that in the WT mice

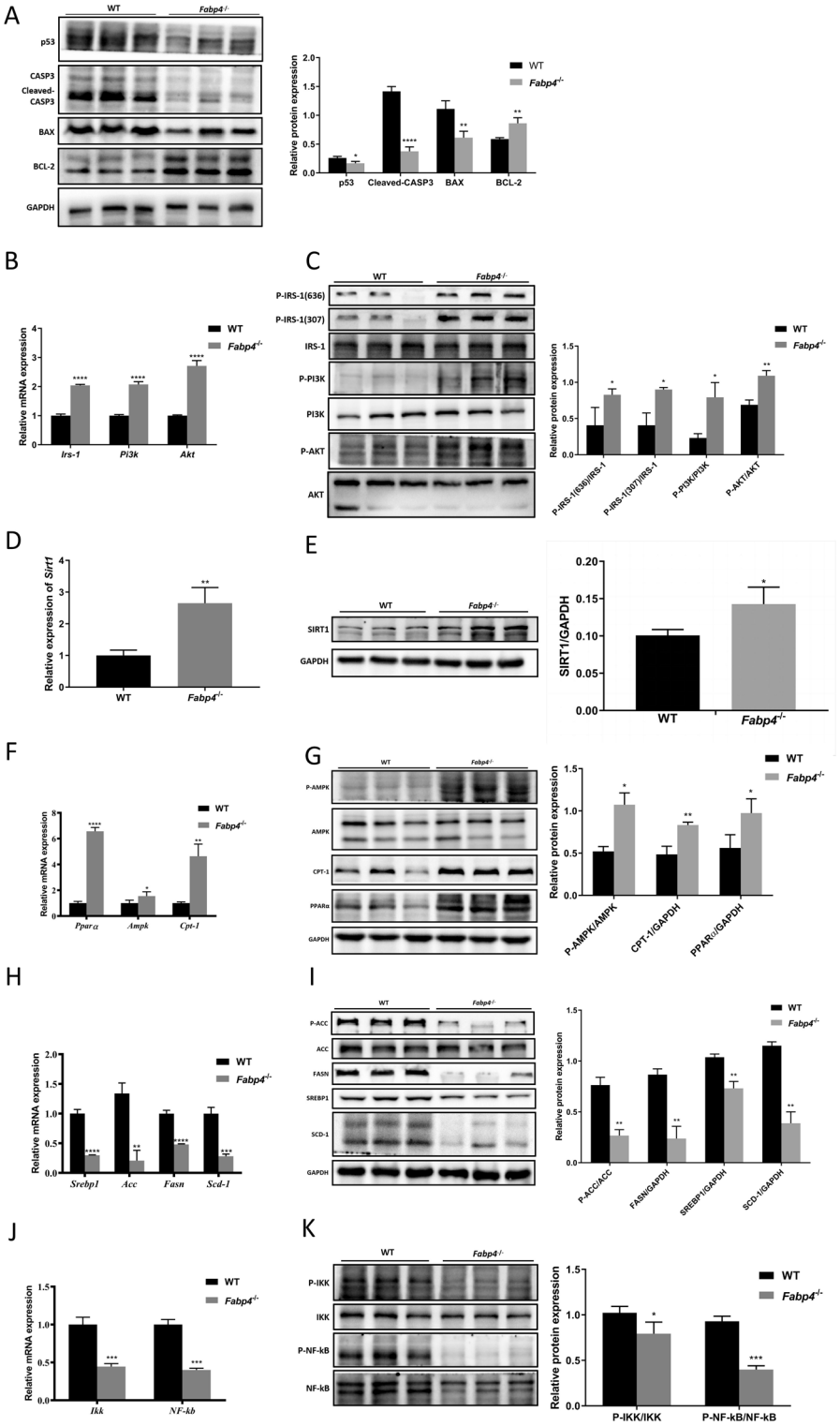

Fig. 6. Expression analysis of the p53 pathway, insulin/PI3K/AKT pathway, and SIRT1 pathway-related molecules in the EtOH-fed WT and *Fabp4*$^{-/-}$ mice. (**A**) Protein levels of p53, CASP3, BAX, and BCL-2 in the EtOH-fed WT and *Fabp4*$^{-/-}$ mice. (**B**) mRNA levels of *Irs-1*, *Pi3k*, and *Akt* in the EtOH-fed WT and *Fabp4*$^{-/-}$ mice. (**C**) Protein levels of P-IRS-1 (636), P-IRS-1 (307), P-PI3K, and P-AKT in the EtOH-fed WT and *Fabp4*$^{-/-}$ mice. (**D**) Hepatic mRNA levels of *Sirt1* in the EtOH-fed WT and *Fabp4*$^{-/-}$ mice. (**E**) Hepatic protein levels of SIRT1 in the EtOH-fed WT and *Fabp4*$^{-/-}$ mice. (**F**) mRNA levels of *Cpt-1*, *Ampk*, and *Pparα* in the EtOH-fed WT and *Fabp4*$^{-/-}$ mice. (**G**) Protein levels of CPT-1, P-AMPK, and PPARα in the EtOH-fed WT and *Fabp4*$^{-/-}$ mice. (**H**) mRNA levels of *Acc*, *Fasn*, *Srebf1*, and *Scd-1* in the EtOH-fed WT and *Fabp4*$^{-/-}$ mice. (**I**) Protein levels of P-ACC, FASN, SREBP1, and SCD-1 in the EtOH-fed WT and *Fabp4*$^{-/-}$ mice. (**J**) mRNA levels of *Ikk* and *Nf-κb* in the EtOH-fed WT and *Fabp4*$^{-/-}$ mice. (**K**) Protein levels of P-IKK and P-NF-κB in the EtOH-fed WT and *Fabp4*$^{-/-}$ mice. Results are presented as the mean ± SD. $^{*}P < 0.05$, $^{**}P < 0.01$, and $^{***}P < 0.001$.

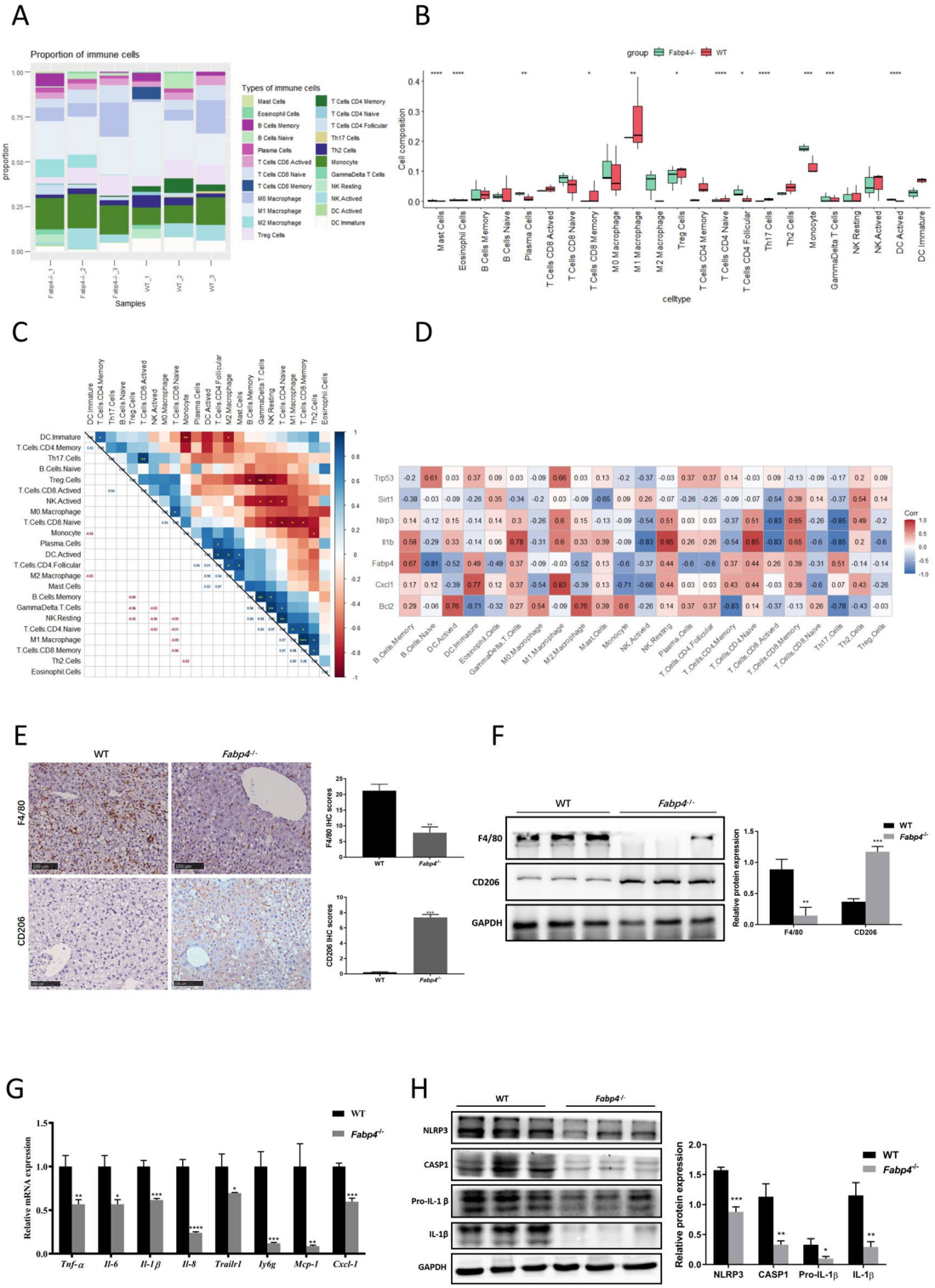

Fig. 7. Correlation analysis between FABP4 expression and macrophage levels in the EtOH-fed WT and *Fabp4*$^{-/-}$ mice. (**A**) Stacked bar chart showing the immune cells in the EtOH-fed WT and *Fabp4*$^{-/-}$ mice. (**B**) Box-plot of the proportion of 23 types of immune cells in the EtOH-fed WT and *Fabp4*$^{-/-}$ mice. (**C**) Heatmap of the correlation between the 23 immune cell types in the EtOH-fed WT and *Fabp4*$^{-/-}$ mice. (**D**) Heatmap of the correlation between infiltrating immune cells and *p53*, *Sirt1*, *Nlrp3*, *Il1b, Fabp4*, *Cxcl1*, and *Bcl-2* in the EtOH-fed WT and *Fabp4*$^{-/-}$ mice. (**E**) Immunohistochemistry staining of F4/80 and CD206 proteins in the EtOH-fed WT and *Fabp4*$^{-/-}$ mice. (**F**) Hepatic protein levels of F4/80 and CD206 in the EtOH-fed WT and *Fabp4*$^{-/-}$ mice. (**G**) Hepatic mRNA levels of *Tnf-α*, *Il-6*, *Il-1β*, *Il-8*, *Trailr1*, *Iy6g*, *Mcp-1*, and *Cxcl-1* in the EtOH-fed WT and *Fabp4*$^{-/-}$ mice. (**H**) Protein levels of NLRP3, CASP1, pro-IL-1β, and IL-1β in the EtOH-fed WT and *Fabp4*$^{-/-}$ mice. Results are presented as the mean ± SD. $^{*}P < 0.05$, $^{**}P < 0.01$, and $^{***}P < 0.001$.

(Fig. 7H). These results suggest that *Fabp4* deficiency may prevent liver inflammation in ASH mice by increasing the proportion of M2 macrophages.

Discussion

ALD significantly contributes to the global burden of disease and mortality[25]. Moreover, ASH can further develop into more severe liver diseases, severely harming the liver and other organs[3]. In this study, we explored the role and underlying mechanisms of FABP4 in ASH progression. Integrative bioinformatics analysis showed that *FABP4* was upregulated in the AH samples of the GSE142530 and GSE167308 datasets. Furthermore, the expression of *FABP4* was found to be upregulated in the liver tissues of AH patients and ASH mice. Interestingly, the serum levels of FABP4 were not significantly different between the EtOH-fed and CD-fed WT mice. Moreover, *Fabp4* deficiency alleviated hepatic steatosis and inflammation in the EtOH-fed *Fabp4*$^{-/-}$ mice. These results suggest that hepatic *Fabp4* expression may play a crucial role in ASH progression. Additionally, our results revealed that *Fabp4* deficiency may inhibit lipogenesis, promote fatty acid oxidation, and facilitate M2 macrophage polarization by suppressing the p53 signaling pathway and activating the SIRT1 signaling pathway in the liver of ASH mice. Therefore, FABP4 may be a potential drug development target for ASH.

Our study found that *FABP4* expression was correlated with AH progression and that the DEGs in the GSE142530 and GSE167308 datasets were significantly enriched in lipid metabolism, immunity, and inflammation. Additionally, our results demonstrated that *FABP4* expression may play a crucial role in hepatic lipid metabolism and inflammation in AH. In addition, ROC analysis and machine learning algorithms (RF, SVM, and XGBoost) revealed that high *FABP4* expression could serve as an effective predictive biomarker for AH, indicating its potential clinical application in AH prediction.

FABP4 plays an essential regulatory role in energy metabolism and inflammatory response[7]. It is associated with several diseases and is a reliable biomarker for aging. FABP4 knockdown promotes cholesterol and fatty acid degradation and reduces inflammation and metabolic disorders in the liver[26]. Additionally, FABP4 promotes M1 macrophage polarization by activating the NF-κB/p65 signaling pathway in nonalcoholic fatty liver disease[27]. Moreover, studies have shown that FABP4 could help to predict poor outcomes in patients with nonalcoholic fatty liver[28]. However, another study found that serum FABP4 levels do not increase in patients with NASH or fibrosis and that the increased hepatic expression of FABP4 may not contribute significantly to the circulating FABP4 levels[29]. In the present study, we found that the serum FABP4 levels did not vary significantly between the EtOH-fed and CD-fed mice; however, the hepatic mRNA and protein levels of FABP4 were increased in the EtOH-fed mice compared with those in the CD-fed mice. Furthermore, our study found that *Fabp4* deletion reduced hepatic lipid deposition and inflammation in the EtOH-fed *Fabp4*$^{-/-}$ mice. Therefore, our results indicate that the hepatic FABP4 levels, but not the serum FABP4 levels, may play a dominant role in ASH progression.

We further explored the underlying mechanisms of FABP4-mediated progression of ASH. Multiple enrichment analyses of the transcription profiling data revealed that the p53 signaling pathway, insulin resistance, and the PI3K-AKT signaling pathway were enriched in the EtOH-fed *Fabp4*$^{-/-}$ and WT mice. Several studies have shown that *p53* plays an vital role in regulating lipid metabolism[30,31]. A study found that the inhibition of p53 transcriptional activity in the livers of high-fat diet mice reduces diet-induced weight gain, hepatic steatosis, oxidative stress, and apoptosis[17]. Derdak et al.[32] found that p53 activation induces various forms of cell death, regulates cellular energy metabolism, and suppresses the insulin/PI3K/AKT axis, contributing to metabolic abnormalities in ALD rats. Our results showed that *Fabp4* deficiency downregulated the expression of *p53* in the liver of ASH mice. A study reported that p53 inhibition upregulates hepatic SIRT1 expression, which further upregulates the expression of PPARα, AMPK, and CPT1 and promotes the β-oxidation of hepatic fatty acids[17–19]. Other studies reported that p53 inhibition increases SIRT1 expression, which downregulates the expression of SREBP1, FASN, SCD-1, and ACC, thereby inhibiting the de novo synthesis of hepatic fatty acids[17,33]. Our results showed that *Fabp4* deficiency upregulated the expression of SIRT1, subsequently reducing lipid synthesis and promoting lipolysis. SIRT1 regulates downstream inflammatory pathways, such as the IKK/NF-κB pathway, and directly affects the expression of inflammatory factors[20,34]. Our study showed that the expression of the IKK/NF-κB pathway-associated factors was decreased in the *Fabp4*$^{-/-}$ mice. These results demonstrate that *Fabp4* deficiency may alleviate hepatic steatosis and inflammation via the p53/PI3K/AKT/SIRT1 signaling pathway; however, further exploration is required to determine its underlying mechanisms.

Considering the essential role of the immune system in AH, we further analyzed the association between *FABP4* expression and immune cells in the AH datasets. The results showed that *FABP4* exhibited varying degrees of correlation with immune cells, such as macrophages and T follicular helper cells. The results were further verified by the GSEA of DEGs obtained from the GSE73173 dataset. Furthermore, the CIBERSORT analysis showed that *Fabp4* was negatively correlated with M2 macrophages. Consistently, the proportion of hepatic M2 macrophages was significantly higher in the *Fabp4*$^{-/-}$ mice than in the WT mice. Moreover, the proportion of inflammation-associated factors was reduced in the *Fabp4*$^{-/-}$ mice. These results provide novel insights into the immune mechanism of FABP4-mediated progression of ASH; however, further research is required to determine the effects of FABP4 expression on macrophage polarization in ASH.

In summary, the present study demonstrates that *Fabp4* deficiency alleviated hepatic lipid accumulation and inflammation in ASH mice. Additionally, our study suggests that the inhibition of FABP4 may be a potential therapeutic strategy for ASH.

Data availability

Sequence data related to this study have been deposited in the NCBI GEO database (https://www.ncbi.nlm.nih.gov/geo/query/acc.cgi?acc=GSE265758), with the GEO series GSE265758.

Received: 19 April 2024; Accepted: 27 August 2024
Published online: 10 September 2024

References

1. Asrani, S. *et al.* Reducing the global burden of alcohol-associated liver disease: A blueprint for action. *Hepatology* **73**(5), 2039–2050. https://doi.org/10.1002/hep.31583 (2021).
2. Seitz, H. *et al.* Alcoholic liver disease. *Nat. Rev. Dis. Primers* **4**(1), 16. https://doi.org/10.1038/s41572-018-0014-7 (2018).
3. Lackner, C. & Tiniakos, D. Fibrosis and alcohol-related liver disease. *J. Hepatol.* **70**(2), 294–304. https://doi.org/10.1016/j.jhep.2018.12.003 (2019).
4. Hydes, T. *et al.* Treating alcohol-related liver disease from a public health perspective. *J. Hepatol.* **70**(2), 223–236. https://doi.org/10.1016/j.jhep.2018.10.036 (2019).
5. Li, B. *et al.* SnapShot: FABP functions. *Cell* **182**(4), 1066-1066.e1061. https://doi.org/10.1016/j.cell.2020.07.027 (2020).
6. Furuhashi, M. & Hotamisligil, G. Fatty acid-binding proteins: Role in metabolic diseases and potential as drug targets. *Nat. Rev. Drug Discov.* **7**(6), 489–503. https://doi.org/10.1038/nrd2589 (2008).
7. Hotamisligil, G. & Bernlohr, D. Metabolic functions of FABPs—Mechanisms and therapeutic implications. *Nat. Rev. Endocrinol.* **11**(10), 592–605. https://doi.org/10.1038/nrendo.2015.122 (2015).
8. Attal, N. *et al.* Fatty acid binding protein-4 promotes alcohol-dependent hepatosteatosis and hepatocellular carcinoma progression. *Transl. Oncol.* **14**(1), 100975. https://doi.org/10.1016/j.tranon.2020.100975 (2021).
9. Attal, N. *et al.* Role of AMPK-SREBP signaling in regulating fatty acid binding-4 (FABP4) expression following ethanol metabolism. *Biology (Basel)* https://doi.org/10.3390/biology11111613 (2022).
10. Attal, N. *et al.* Cytochrome P450 2E1-dependent hepatic ethanol metabolism induces fatty acid-binding protein 4 and steatosis. *Alcohol Clin. Exp. Res.* **46**(6), 928–940. https://doi.org/10.1111/acer.14828 (2022).
11. Massey, V. *et al.* Integrated multiomics reveals glucose use reprogramming and identifies a novel hexokinase in alcoholic hepatitis. *Gastroenterology* **160**(5), 1725-1740.e1722. https://doi.org/10.1053/j.gastro.2020.12.008 (2021).
12. Bou Saleh, M. *et al.* Loss of hepatocyte identity following aberrant YAP activation: A key mechanism in alcoholic hepatitis. *J. Hepatol.* **75**(4), 912–923. https://doi.org/10.1016/j.jhep.2021.05.041 (2021).
13. Furuhashi, M. *et al.* Local production of fatty acid-binding protein 4 in epicardial/perivascular fat and macrophages is linked to coronary atherosclerosis. *Arterioscler. Thromb. Vasc. Biol.* **36**(5), 825–834. https://doi.org/10.1161/atvbaha.116.307225 (2016).
14. Simran, B., Pooja, & Sudesh Kumar, Y. CRISPR-Cas for genome editing: Classification, mechanism, designing and applications. *Int. J. Biol. Macromol.* https://doi.org/10.1016/j.ijbiomac.2023.124054 (2023).
15. Xu, M. *et al.* Fat-specific protein 27/CIDEC promotes development of alcoholic steatohepatitis in mice and humans. *Gastroenterology* **149**(4), 1030-1041.e1036. https://doi.org/10.1053/j.gastro.2015.06.009 (2015).
16. Edu, J., Johnson, W. E. & Edu, A. Surrogate variable analysis. *Dissert. Theses Gradworks* https://doi.org/10.18129/B9.bioc.sva (2013).
17. Derdak, Z. *et al.* Inhibition of p53 attenuates steatosis and liver injury in a mouse model of non-alcoholic fatty liver disease. *J. Hepatol.* **58**(4), 785–791. https://doi.org/10.1016/j.jhep.2012.11.042 (2013).
18. Pawlak, M., Lefebvre, P. & Staels, B. Molecular mechanism of PPARα action and its impact on lipid metabolism, inflammation and fibrosis in non-alcoholic fatty liver disease. *J. Hepatol.* **62**(3), 720–733. https://doi.org/10.1016/j.jhep.2014.10.039 (2015).
19. Zhang, N. *et al.* Fenofibrate treatment attenuated chronic endoplasmic reticulum stress in the liver of nonalcoholic fatty liver disease mice. *Pharmacology* **95**, 173–180. https://doi.org/10.1159/000380952 (2015).
20. Kauppinen, A. *et al.* Antagonistic crosstalk between NF-κB and SIRT1 in the regulation of inflammation and metabolic disorders. *Cell Signal.* **25**(10), 1939–1948. https://doi.org/10.1016/j.cellsig.2013.06.007 (2013).
21. Weichselbaum, L. *et al.* Epigenetic basis for monocyte dysfunction in patients with severe alcoholic hepatitis. *J. Hepatol.* **73**(2), 303–314. https://doi.org/10.1016/j.jhep.2020.02.017 (2020).
22. Gao, B. *et al.* Inflammatory pathways in alcoholic steatohepatitis. *J. Hepatol.* **70**(2), 249–259. https://doi.org/10.1016/j.jhep.2018.10.023 (2019).
23. Liao, M. *et al.* Single-cell landscape of bronchoalveolar immune cells in patients with COVID-19. *Nat. Med.* **26**(6), 842–844. https://doi.org/10.1038/s41591-020-0901-9 (2020).
24. Erbay, E. *et al.* Reducing endoplasmic reticulum stress through a macrophage lipid chaperone alleviates atherosclerosis. *Nat. Med.* **15**(12), 1383–1391. https://doi.org/10.1038/nm.2067 (2009).
25. Lee, B. *et al.* National trends and long-term outcomes of liver transplant for alcohol-associated liver disease in the United States. *JAMA Intern. Med.* **179**(3), 340–348. https://doi.org/10.1001/jamainternmed.2018.6536 (2019).
26. Jian, L. *et al.* Targeting FABP4 in elderly mice rejuvenates liver metabolism and ameliorates aging-associated metabolic disorders. *Metabolism* https://doi.org/10.1016/j.metabol.2023.155528 (2023).
27. Cui, Z. *et al.* FABP4 in LSECs promotes CXCL10-mediated macrophage recruitment and M1 polarization during NAFLD progression. *Biochim. Biophys. Acta Mol. Basis Dis.* https://doi.org/10.1016/j.bbadis.2023.166810 (2023).
28. Audrey, C. *et al.* FABP4 and MMP9 levels identified as predictive factors for poor prognosis in patients with nonalcoholic fatty liver using data mining approaches and gene expression analysis. *Sci. Rep.* https://doi.org/10.1038/s41598-019-56235-y (2019).
29. Jonas, W. *et al.* Fatty acid-binding protein-4 (FABP4) and matrix metalloproteinase-9 (MMP9) as predictive values for nonalcoholic steatohepatitis (NASH). *Lipids Health Dis.* https://doi.org/10.1186/s12944-022-01764-1 (2023).
30. Vousden, K. & Ryan, K. p53 and metabolism. *Nat. Rev. Cancer* **9**(10), 691–700. https://doi.org/10.1038/nrc2715 (2009).
31. Liu, Y. & Gu, W. The complexity of p53-mediated metabolic regulation in tumor suppression. *Semin. Cancer Biol.* **85**, 4–32. https://doi.org/10.1016/j.semcancer.2021.03.010 (2022).
32. Derdak, Z. *et al.* Activation of p53 enhances apoptosis and insulin resistance in a rat model of alcoholic liver disease. *J. Hepatol.* **54**(1), 164–172. https://doi.org/10.1016/j.jhep.2010.08.007 (2011).
33. Nogueiras, R. *et al.* Sirtuin 1 and sirtuin 3: Physiological modulators of metabolism. *Physiol. Rev.* **92**(3), 1479–1514. https://doi.org/10.1152/physrev.00022.2011 (2012).
34. Castro, R. *et al.* miR-34a/SIRT1/p53 is suppressed by ursodeoxycholic acid in the rat liver and activated by disease severity in human non-alcoholic fatty liver disease. *J. Hepatol.* **58**(1), 119–125. https://doi.org/10.1016/j.jhep.2012.08.008 (2013).

Author contributions

Fudi Zhong and Keqing Jiang designed and supervised the experiment and revised the manuscript. Hao Xing performed some experiments and wrote the manuscript; Zhan Wu, Shuiping Yu, Guandou Yuan, Zhenya Guo and Songqing He participated in some experiments and analyzed some data.

Funding

National Key Research and Development Program (2022YFE0131600); Joint Project on Regional High-Incidence Diseases Research of Guangxi Natural Science Foundation (2023GXNSFAA026062); National Natural Science Foundation of China (82160120); Natural Science Foundation of Guangxi Province (2021GXNSFDA075002);

the "111" Project (D17011); Advanced Innovation Teams and Xinghu Scholars Program of Guanxi Medical University; Innovation Team of the First Affiliated Hospital of Guangxi Medical University (YYZS2022002).

Competing interests
The authors declare no competing interests.

Additional information
Supplementary Information The online version contains supplementary material available at https://doi.org/10.1038/s41598-024-71311-8.

Correspondence and requests for materials should be addressed to S.H. or F.Z.